Sixth International Symposium on Marine Propulsors
smp'19, Rome, Italy, May 2019

Large Eddy Simulation of flow over a confined elliptic hydrofoil*

Praveen Kumar[1], **Krishnan Mahesh**[1]

[1]Department of Aerospace Engineering & Mechanics, University of Minnesota, Minneapolis, USA

ABSTRACT

Large-eddy simulation (LES) is used to study the evolution of the tip vortex generated by a three-dimensional elliptical hydrofoil at 12 degrees angle of attack and a Reynolds number of 9×10^5 based on root chord length and freestream velocity. The simulations are based on the experiments of Boulon et al. (1999), who studied the effect of confinement on tip vortex cavitation by varying the perpendicular distance between the tip and the bottom wall. The present simulations correspond to their case where the confinement due to the bottom wall is negligible. Results are compared to the available experimental data showing reasonable agreement. The tip vortex undergoes spiral roll-up whereas the trailing edge wake shows progressive bending moving downstream, due to the confinement effect of the side walls. The spiral length scale varies linearly with the downstream distance up to the length of the simulated domain. Future work will focus on comparing the present results to a highly confined case of Boulon et al. (1999).

Keywords LES, tip vortex, elliptic hydrofoil.

1 INTRODUCTION

The structure and development of the tip vortex formed behind a wing has been the subject of many papers (see Devenport et al. (1996) and the references therein). The tip vortex formed by a finite span hydrofoil has been widely studied due to its relevance to marine propulsors. In many cases, the tip vortex can cavitate depending on the physical conditions, and the prediction of cavitation inception is challenging for such flows. Tip vortices have been studied by several researchers as reviewed by Arndt (2002). The behavior of tip vortices is significantly altered in the presence of confinement, which is typically encountered in ducted propulsors and turbomachinery. Liu et al. (2018) reviewed recent work on the effect of tip clearance on the flow field of propellers and turbomachinery.

In this paper, we simulate the flow configuration of Boulon et al. (1999), who studied flow over a three-dimensional elliptical hydrofoil NACA 16-020 at various angles of attack and Reynolds number (Re). Confinement was achieved by a flat wall with tip clearance (e). Boulon et al. (1999) varied e and characterized the resultant flow field in terms of its cavitation behavior. Some of the main conclusions of their work are:

- The turbulent boundary on the confinement plate does not interact with the tip vortex.
- The value of e significantly affects vortex structure and hence, cavitation inception. As e becomes smaller, the tip vortex becomes more susceptible to cavitation up to a certain value of e due to increase in the peak of swirl velocity. Beyond that, decreasing e does not cavitate the flow because of increase in the core radius thereby decreasing the peak of swirl velocity.
- The tangential velocity profile is highly asymmetric in the near field but becomes more symmetric moving downstream.
- For confined tip vortex flow, the inception cavitation number does not correlate with lift coefficient, but varies as square of circulation.

The present work is focused on the non-cavitating flow over the hydrofoil. This problem has two major challenges: (i) flow over the hydrofoil and (ii) interaction of the tip vortex with walls. Flow over the hydrofoil is computationally challenging due to high Re which demands fine resolution near wall to capture boundary layer. Moreover, the flow can separate on the suction side of the blade due to large angle of attack, causing large unsteadiness. The confinement enhances unsteadiness further. The tip vortex has a tiny core which needs to be resolved throughout the length of the simulation domain. As the tip vortex evolves, the vorticity and turbulence in the core decays. Thus, this problem demands an accurate and robust numerical method which capture the essential flow features. Direct numerical simulation (DNS) of the flow is not feasible for this problem. Thus, large eddy simulation (LES) technique is used to simulate this problem due to its predictive capability for a variety of complex marine flow problems of interest (Mahesh et al., 2015).

Mahesh et al. (2004) developed a non-dissipative and robust finite volume method for large eddy simulation (LES) on unstructured grids, which has been used to accurately simulate a variety of marine flows including flow over hull (Kumar and Mahesh, 2018) and propeller in both crashback (Verma et al., 2012; Jang and Mahesh, 2013; Jang et al., 2012) and forward (Kumar and Mahesh, 2017) modes. The high-fidelity flow field of propeller in forward (design) mode of operation obtained by Kumar and Mahesh (2017) was subsequently used by Keller et al. (2018) to compute and examine far-field sound generated by the propeller.

*Email for correspondence: kmahesh@umn.edu

LES is performed for flow over a three-dimensional elliptical hydrofoil NACA 16-020 at an angle of attack of 12 degrees, and $Re = 9 \times 10^5$ based on root chord length (c) and freestream velocity (U_∞) using the algorithm of Mahesh et al. (2004). The simulations match the domain and physical parameters of the experiments of Boulon et al. (1999). The problem is computationally challenging due to the high Re of the flow and complexity of the grid generation due to small e. LES has been used in past to study the effect of tip-gap on the flow field in a turbomachinery cascade (e.g. You et al. (2006)). The goals of the present work are : (i) to demonstrate the capability of LES to simulate the flow field, and (ii) to study the evolution of the tip vortex in the presence of confinement. The paper is organized as follows. The simulation details including the numerical method, hydrofoil geometry, computational grid and boundary conditions are described in §2. The results are discussed in §3. Finally, the essential flow physics are summarized in §4 along with plans for future work.

2 SIMULATION DETAILS

2.1 Numerical method

In LES, large scales are directly accounted for by the spatially filtered Navier–Stokes equations, whereas the effect of small scales is modeled. The spatially filtered incompressible Navier–Stokes equations are as follows:

$$\begin{aligned} \frac{\partial \overline{u}_i}{\partial t} + \frac{\partial}{\partial x_j}(\overline{u}_i \overline{u}_j) &= -\frac{\partial \overline{p}}{\partial x_i} + \nu \frac{\partial^2 \overline{u}_i}{\partial x_j \partial x_j} - \frac{\partial \tau_{ij}}{\partial x_j}, \\ \frac{\partial \overline{u}_i}{\partial x_i} &= 0, \end{aligned} \tag{1}$$

where u_i is the velocity, p is the pressure, ν is the kinematic viscosity, the overbar $\overline{(.)}$ denotes the spatial filter and $\tau_{ij} = \overline{u_i u_j} - \overline{u}_i \overline{u}_j$ is the sub-grid stress. The dynamic Smagorinsky model proposed by Germano et al. (1991) and modified by Lilly (1992) is used to model the sub-grid stress terms. The Lagrangian time scale is dynamically computed based on surrogate–correlation of the Germano–identity error (Park and Mahesh, 2009). This approach extended to unstructured grids has shown good performance for a variety of flows (Verma and Mahesh, 2012).

Eq. (1) is solved by a numerical method developed by Mahesh et al. (2004) for incompressible flows on unstructured grids. The algorithm is derived to be robust without any numerical dissipation. It is a finite volume method where the Cartesian velocities and pressure are stored at the centroids of the cells and the face normal velocities are stored independently at the centroids of the faces. A predictor–corrector approach is used. The predicted velocities at the control volume centroids are first obtained and then interpolated to obtain the face normal velocities. The predicted face normal velocity is projected so that the continuity equation in Eq. (1) is discretely satisfied. This yields a Poisson equation for pressure which is solved iteratively using a multigrid approach. The pressure field is used to update the Cartesian control volume velocities using a least-square formulation. Time advancement is performed using an implicit Crank–Nicholson scheme. The algorithm has been validated for a variety of problems over a range of Re as described in Section 1.

2.2 Hydrofoil geometry, computational grid and boundary conditions

The hydrofoil has a NACA 16-020 cross-section and an elliptical planform of span $S = 0.18m$ and a root chord length $c = 0.12m$. The aspect ratio is 3.8. The hydrofoil is mounted such that the mid point of the root chord of the hydrofoil is the origin of the Cartesian coordinate system and the tip is located at (0,-S, 0). The hydrofoil span aligns with the y axis and x is the downstream streamwise direction. The two side walls are located at $z = \pm L_z/2$, where $L_z = 0.175$. Note that one grid unit is equivalent to 1 m length in the reference experiment. Hence, the tip-gap $e = 0.06$ which corresponds to the experimental setup of $e = 60$ mm, is generally chosen as the reference case corresponding to no confinement due to the bottom wall. As stated in the reference paper, the two side walls cause confinement resulting in a 27% increase of lift. The Re based on c and U_∞ is 9×10^5 and the hydrofoil is rotated about y to make an angle of attack of 12 degrees. The inflow and outflow planes are located at $L_{up} = 2.58c$ upstream and $L_{dn} = 4.92c$ downstream of the tip respectively. The schematic of the computational domain is shown in Figure 1.

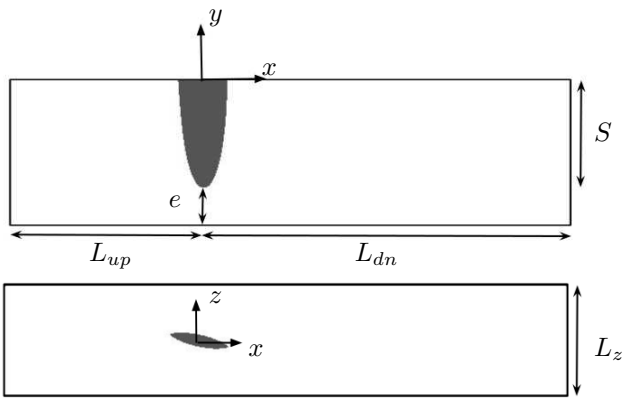

Figure 1: Schematic of the computational domain shown in $z = 0$ (a) and $y = 0.1$ (b) planes.

Freestream velocity is prescribed at the inflow and convective boundary conditions are applied at the outflow. All other domain boundaries have no-slip boundary conditions. A coarse grid (not shown here) of 18 million hexahedral control volumes is first used to access grid resolution and obtain a solution which is used to initialize fine grid simulation. The fine grid containing 97 million hexahedral control volumes is nominally 2 times finer in each direction compared to the coarse grid everywhere except near wall (no-slip) boundaries. The span of the hydrofoil has more than 320 cells and there are more than 400 cells in z direction for the fine grid. The gap between tip of the hydrofoil and the bottom wall contains more than 150 cells. The grid is clustered near all the wall boundaries with a

nominal wall-normal first cell size of $6.67 \times 10^{-4}c$ and $1.67 \times 10^{-3}c$ at hydrofoil surface and other walls respectively with a growth rate of one percent. The computational time step $\Delta t U_\infty / c = 1.67 \times 10^{-5}$ is used for the simulations reported in this paper. All the results presented in this paper are normalized appropriately using U_∞ and c.

3 RESULTS

3.1 Instantaneous flow field

The hydrofoil wake consists of trailing edge wake vortices connected to a tip vortex which is shed from the tip of the hydrofoil. The coherent vortical structures in the wake are visualized using the isocontour of λ_2 (Jeong and Hussain, 1995) colored with pressure as shown in Figure 2. Note that the bottom and side walls removed for clear visualization. The suction side of the blade can be seen to have flow separation leading to the formation of the vortical structures in the wake. The tip vortex remains coherent throughout the simulated domain.

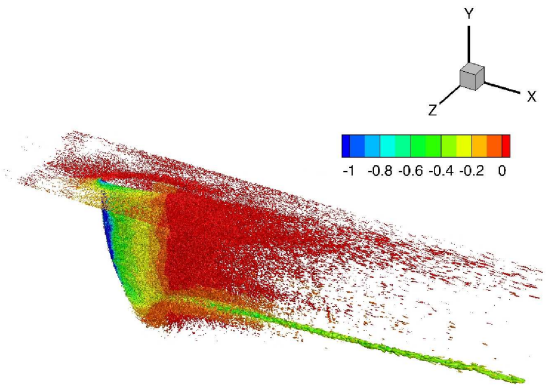

Figure 2: Isocontour of λ_2 colored with pressure showing the trailing edge wake and the tip vortex. The bottom and side walls are removed for visualization.

Figure 3 shows the instantaneous pressure, streamwise velocity and vorticity magnitude in $z = 0$ plane. The tip vortex is visible clearly as the region of low pressure and high vorticity. The pressure minimum at a given downstream location occurs in the core of tip vortex, which decreases moving downstream. The streamwise velocity field shows shear layers in the wake, with a small region of flow separation near the trailing edge. Figure 3c shows that there are three main regions of high vorticity: the tip vortex, the trailing edge and the boundary layers on the no-slip boundaries. In order to have a closer look at the flow, the pressure and streamwise velocity fields are also shown in $y/c = -0.83$ plane in Figure 4. The flow seems to have a small separation region near the leading edge, followed by a reattachment and an eventual separation in the second half of the chord to form wake. The flow separation at the leading edge may be a consequence of the sharp leading edge subjected to a high angle attack.

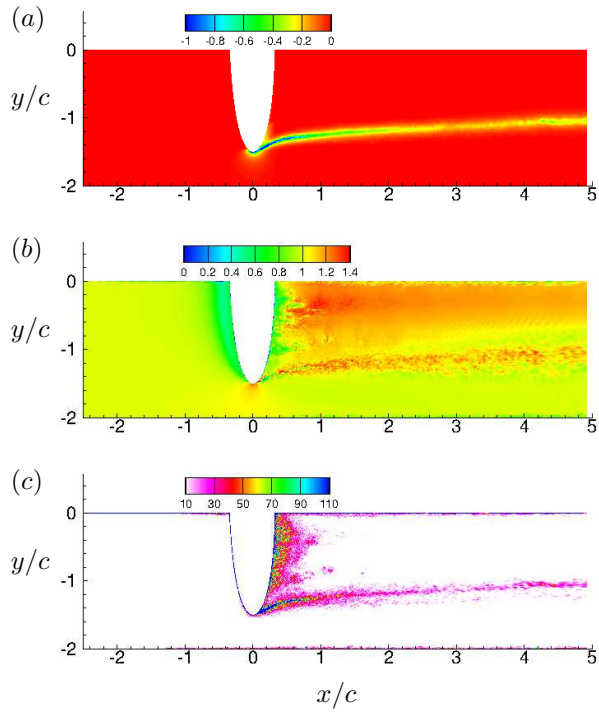

Figure 3: Instantaneous flow field showing pressure (a), streamwise velocity (b) and vorticity magnitude (c) in $z = 0$ plane.

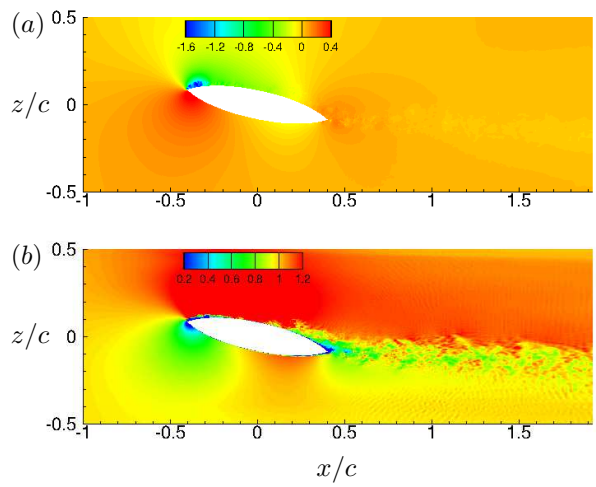

Figure 4: Instantaneous flow field showing pressure (a) and streamwise velocity (b) in $y/c = -0.83$ plane.

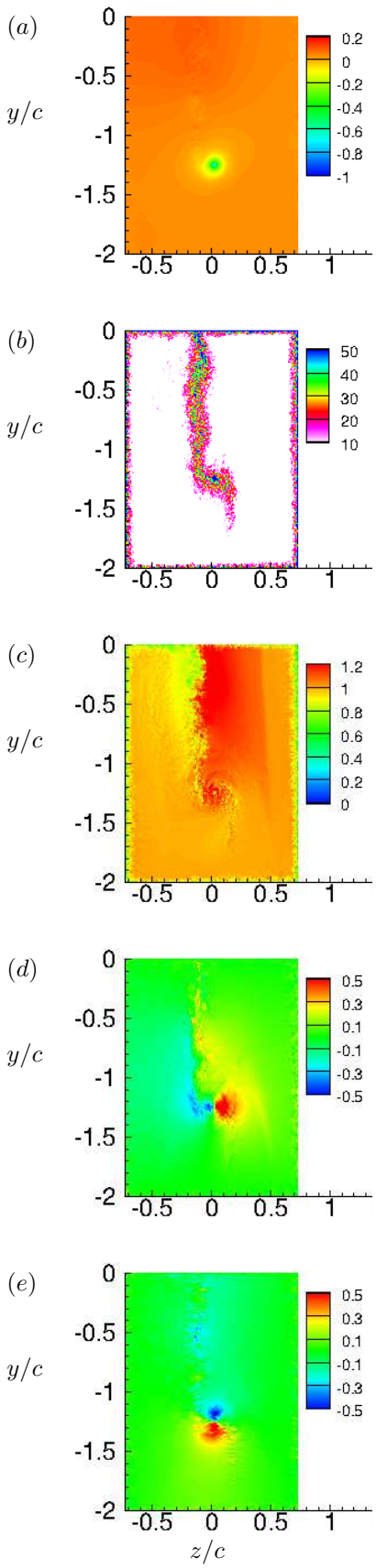

Figure 5: Instantaneous flow field showing pressure (a), vorticity magnitude (b) and the velocity components in x (c), y (d) and z (e) directions at $x/c = 1$.

The instantaneous flow field quantities at a streamwise location $x/c = 1$ are shown Figure 5. The tip vortex is observed as the local minimum of pressure. The overall wake appears as a line of vortex ending up into a tip vortex, which undergoes the process of spiral roll-up in counterclockwise sense in the figure shown. The boundary layers on all the wall boundaries can be observed. The Cartesian velocity components show that the velocity jumps accross the shear layer. The existence of this high axial velocity near the axis of symmetry distinguishes the trailing edge vortices from other types of line vortices (Batchelor, 1964).

3.2 Time-averaged flow field

The instantaneous flow fields are time-averaged after one flow-through time to obtain mean flow field. Figure 6 shows components of mean velocity in $z = 0$ plane. The shear layer appears to grow in the y direction in all the components moving downstream. The region in the vicinity of the tip has large magnitude of tangential velocity mainly due to the end effects where the flow tends to move from the pressure side to the suction side. The spanwise component of mean velocity shows the mean swirl of the axial tip vortex.

Figure 7 shows components of turbulent intensity at $x/c = 1$. The axial component dominates the wall boundary layers whereas all the components are of same order for the wake. The boundary layer of the bottom wall is far away from the tip vortex core.

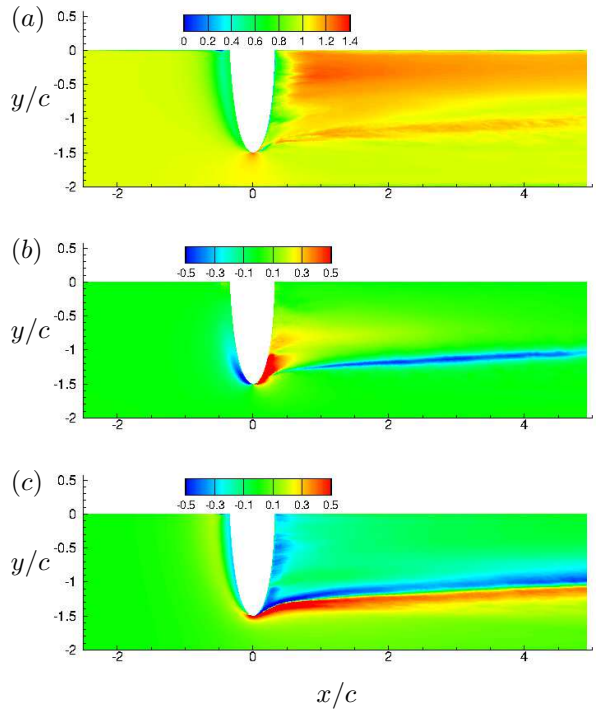

Figure 6: Mean velocity components in axial (a), tangential (b) and spanwise (c) directions are shown in $z = 0$ plane.

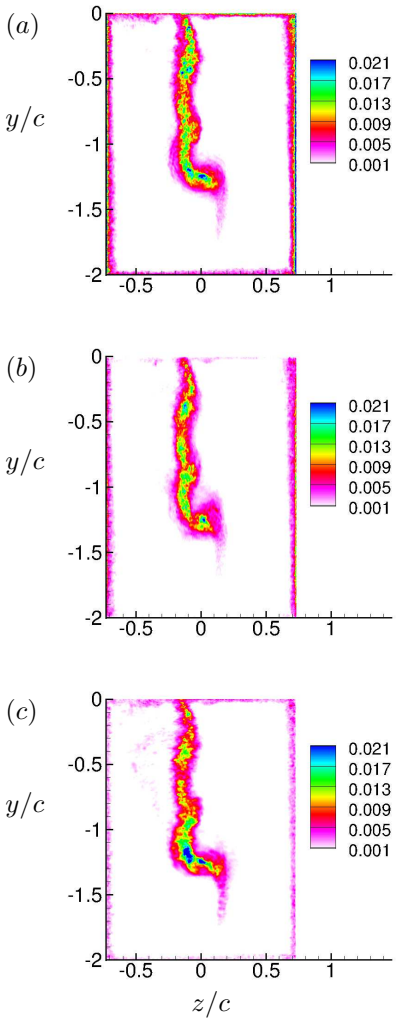

Figure 7: Turbulent intensities in streamwise (a), tangential (b) and spanwise (c) directions are shown at $x/c = 1$.

3.3 Comparison to experiment

Boulon et al. (1999) provides the measured profiles of mean (V) and r.m.s (V_{rms}) of tangential velocity at $x/c = 1$ for the case simulated in the present paper. Figure 8 shows profiles of both these quantities along with the experimental data. Note that the simulation results are shown in the coordinate system adopted in the experiments. The results show reasonable agreement away from the tip vortex core for both quantities. The sharp jump in tangential velocity across the core and its r.m.s value at the core center is smaller compared to the experiment. Possible reasons for this observation can be the grid resolution and the statistical convergence. Both these factors are currently being explored in the ongoing work. Unfortunately, the velocity field measurements at other locations in the wake are not reported.

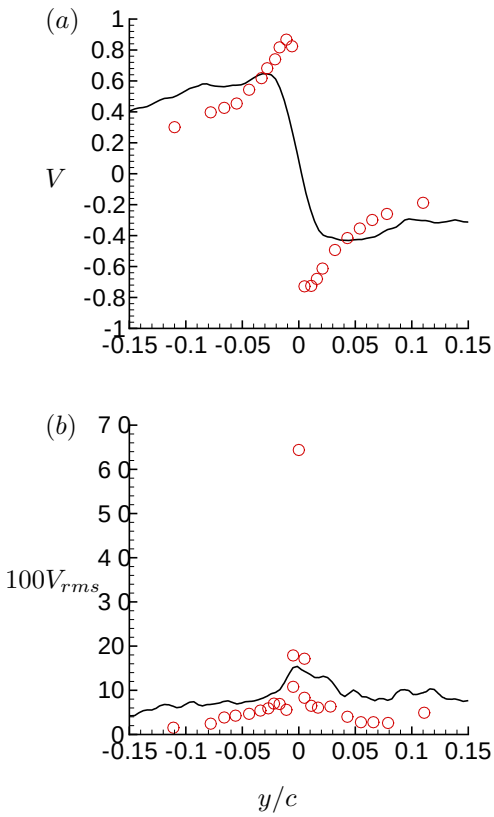

Figure 8: LES results compared to the experiments (Boulon et al., 1999) for mean (a) and r.m.s. (b) of tangential velocity at $x/c = 1$.

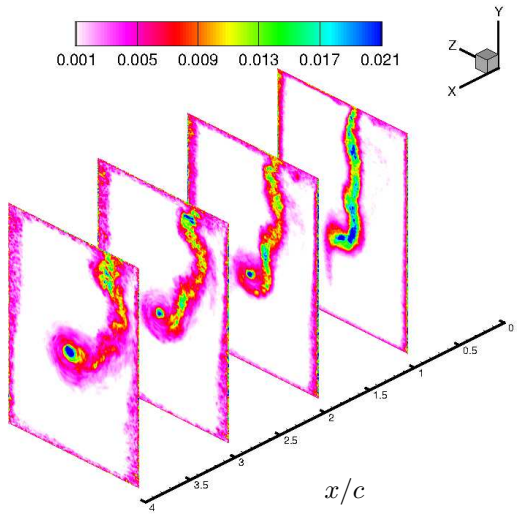

Figure 9: TKE at various downstream locations in the wake.

3.4 Axial evolution of the tip vortex

The axial evolution of the tip vortex is visualized in Figure 9 by showing contours of TKE at multiple locations downstream of the hydrofoil. The progressive spiral roll-up of the tip vortex along with bending of the trailing edge wake

can be observed, as the wake evolves downstream. This behavior of the wake is different than the wake behavior when there is no confinement due to side-walls, e.g. the finite wing tip vortex experimentally studied by Devenport et al. (1996).

Devenport et al. (1996) studied the wake of a finite wing with NACA0012 crossection and a rounded tip at comparable Re. They report measurements from 5 to 25 chords downstream and analyzed the wake behavior in terms of the nature of the vortex core and its self-similar evolution. They observed the spiral roll-up of the tip vortex without any bending of the trailing edge wake. They defined a spiral length scale (ζ) as the spanwise separation between the tip vortex core and the centerline of the trailing edge wake. When scaled with (ζ, they showed that the locus of maxima of axial turbulent intensity collapsed for all the measured wake locations. Moreover, ζ was found to vary as $\sqrt{x}$ from 5-25 chord lengths.

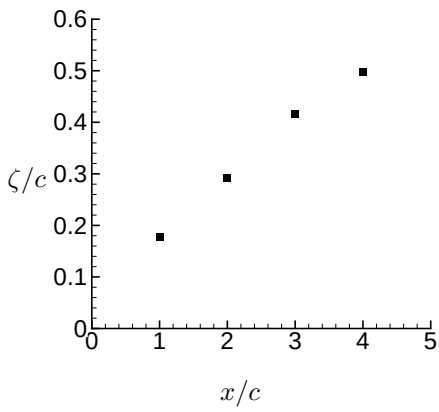

Figure 10: Streamsiwse evolution of the spiral length scale (ζ).

For the present case however, the trailing edge wake no longer remain straight moving downstream, due to the confinement effect of the side walls. So, the definition of ζ is modified as the separation between the tip vortex core and the centerline of the trailing edge wake near root. Figure 10 shows the streamwise evolution of ζ. Note that the presented results show the streamwise evolution of ζ in the near field compared to that reported by Devenport et al. (1996). The variation of ζ is almost linear for the length of the simulated domain.

4 SUMMARY

Wall-resolved LES is used to simulate flow over a three-dimensional elliptical hydrofoil at 12 degrees angle of attack and $Re = 9 \times 10^5$ based on root chord length and freestream velocity. The simulations are based on the experiments of Boulon et al. (1999), who studied the effect of confinement on tip vortex cavitation and the present case match their case where the flow confinement due to the bottom wall is negligible. Profiles of mean and r.m.s of the tangential velocity at $x/c = 1$ show reasonable agreement with the experimental data.

The flow field is described in terms of instantaneous and mean behavior. The flow separates on the suction side to form trailing edge wake appearing as a line vortex culminating in a tip vortex. The spiral roll-up of the tip vortex is accompanied by the progressive bending of the trailing edge wake as the flow evolves downstream. The spiral length scale varies linearly up to the length of the simulated domain.

The ongoing and future work include simulating even finer grid for the present case to ensure grid convergence. Simulations are also ongoing for the highly confined case ($e = 1.9\ mm$) of Boulon et al. (1999). The results will be compared to the available experimental data and the flow field will be analyzed with respect to key differences compared to the case reported in this paper.

ACKNOWLEDGEMENTS

This work is supported by the United States Office of Naval Research (ONR) under ONR Grant N00014-17-1-2676 with Dr. Ki-Han Kim as technical monitor. The computations were made possible through the resources provided by the High Performance Computing Modernization program (HPCMP) and the Minnesota Supercomputing Institute (MSI). The authors thank Mr. Karim Alamé for his help with the generation of the hydrofoil geometry.

REFERENCES

Arndt, R. E. A. "Cavitation in vortical flows". Annual Review of Fluid Mechanics, 34(1):143–175, 2002.

Batchelor, G. K. "Axial flow in trailing line vortices". Journal of Fluid Mechanics, 20(4):645–658, 1964.

Boulon, O., Callenaere, M., Franc, J.-P., and Michel, J.-M. "An experimental insight into the effect of confinement on tip vortex cavitation of an elliptical hydrofoil". Journal of Fluid Mechanics, 390:1–23, 1999.

Devenport, W. J., Rife, M. C., Liapis, S. I., and Follin, G. J. "The structure and development of a wing-tip vortex". Journal of Fluid Mechanics, 312:67–106, 1996.

Germano, M., Piomelli, U., Moin, P., and Cabot, W. H. "A dynamic subgrid–scale eddy viscosity model". Physics of Fluids A, 3:7:1760, 1991.

Jang, H. and Mahesh, K. "Large eddy simulation of flow around a reverse rotating propeller". Journal of Fluid Mechanics, 729:151–179, 2013.

Jang, H., Verma, A., and Mahesh, K. "Predicting unsteady loads in marine propulsor crashback using large eddy simulation". International Journal of Rotating Machinery, 2012, 2012.

Jeong, J. and Hussain, F. "On the identification of a vortex". Journal of Fluid Mechanics, 285:69–94, 1995.

Keller, J., Kumar, P., and Mahesh, K. "Examination of propeller sound production using large eddy simulation". Physical Review Fluids, 3(6):064601, 2018.

Kumar, P. and Mahesh, K. "Large eddy simulation of propeller wake instabilities". Journal of Fluid Mechanics,

814:361–396, 2017.

Kumar, P. and Mahesh, K. "Large-eddy simulation of flow over an axisymmetric body of revolution". Journal of Fluid Mechanics, 853:537–563, 2018.

Lilly, D. K. "A proposed modification of the Germano subgrid–scale closure model". Physics of Fluids A, 4:3: 633–635, 1992.

Liu, Y., Tan, L., and Wang, B. "A review of tip clearance in propeller, pump and turbine". Energies, 11(9):2202, 2018.

Mahesh, K., Constantinescu, G., and Moin, P. "A numerical method for large–eddy simulation in complex geometries". Journal of Computational Physics, 197:1: 215, 2004.

Mahesh, K., Kumar, P., Gnanaskandan, A., and Nitzkorski, Z. "LES applied to ship research". Journal of Ship Research, 59(4):238–245, 2015.

Park, N. and Mahesh, K. "Reduction of the Germano-identity error in the dynamic Smagorinsky model". Physics of Fluids (1994-present), 21(6):065106, 2009.

Verma, A. and Mahesh, K. "A Lagrangian subgrid-scale model with dynamic estimation of Lagrangian time scale for large eddy simulation of complex flows". Physics of Fluids (1994-present), 24(8):085101, 2012.

Verma, A., Jang, H., and Mahesh, K. "The effect of an upstream hull on a propeller in reverse rotation". Journal of Fluid Mechanics, 704:61–88, 2012.

You, D., Wang, M., Moin, P., and Mittal, R. "Effects of tip-gap size on the tip-leakage flow in a turbomachinery cascade". Physics of Fluids, 18(10):105102, 2006.